ACS APPLIED MATERIALS & INTERFACES

Research Article

www.acsami.org

Grafted Carbazole-Assisted Electrodeposition of Graphene Oxide

Joey Dacula Mangadlao,[†] Al Christopher C. De Leon,[†] Mary Jane L. Felipe,[‡] Pengfei Cao,[†] Paul A. Advincula,[†] and Rigoberto C. Advincula*[,†]

[†]Department of Macromolecular Science and Engineering, Case Western Reserve University, Cleveland, Ohio 44106, United States

[‡]Department of Chemistry, University of Houston, Houston, Texas 77204, United States

Supporting Information

ABSTRACT: The electrodeposition of graphene oxide (GO) by covalently linked electroactive monomer, carbazole (Cbz) is first demonstrated herein. This is based on the electropolymerization and electrodeposition of covalently linked Cbz units when a potential is applied. During the electrochemical process, the Cbz groups electropolymerize and carry the GO nanosheets as it electrodeposits on the substrate. Moreover, the GO−Cbz sheets selectively deposit onto the conducting regions of the substrate, which demonstrates its promise for the fabrication of electropatterned graphene-based devices. In addition, GO−Cbz is a promising material for the fabrication of nanocomposite coatings for anticorrosion application. In as little as 1 wt % GO−Cbz loading, a protection efficiency as high as 95.4% was achieved.

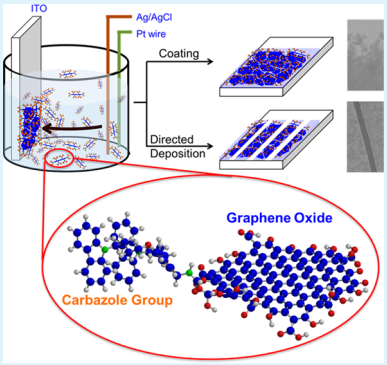

KEYWORDS: *graphene oxide, electrodeposition, carbazole, electropolymerization, corrosion*

INTRODUCTION

A decade after its discovery, graphene, a two-dimensional, one-atom thick carbon nanomaterial, continues to be a subject of research both in the academe and in the industry. This is mainly due to graphene's remarkable electronic properties such as room-temperature Quantum Hall effect and extremely high mobility of its charge carriers (200 000 cm^2 V^{-1} s^{-1}), which open possibilities for ballistic conduction.[1] Graphene is also known for its extraordinary mechanical, thermal, optical, and chemical properties.[2−5] Several applications of graphene have emerged in the area of transparent and flexible electrodes, electromechanical resonators, supercapacitors, plasmonics, high-performance conducting nanocomposites, and even biomedicine.[6−11]

Typically, graphene is fabricated by chemical vapor deposition (CVD). However, solution processes through graphene oxide (GO) are equally explored in literature since it is more amenable to low-cost mass production and more flexible to a myriad of solution-based manufacturing processes such as membrane filtration, Langmuir−Blodgett (LB) assembly, Layer-by-layer (LbL) deposition, dip-coating, spray-coating, spin-coating, and electrophoretic deposition (EPD).[12−17] LB assembly affords the deposition of monolayer-thick GO; however, the tedious process as well as the limited area of the substrate hinders its practical application. Though LbL, dip-coating, spray-coating, and spin-coating are readily applicable to large-area substrates, thickness and uniformity remain issues. More recently, it was reported that EPD effectively offers good thickness controllability and uniformity.[16] However, the process is energy-intensive as it typically requires 10 V DC voltage to force the GO platelets to migrate and deposit toward the positive electrode.

In this contribution, we highlight the synthesis, characterization, and electrodeposition of GO sheets with covalently tethered, electroactive carbazole group (Cbz). The underlying concept relies on the electropolymerization and electrodeposition of Cbz units to metallic substrates when a particular voltage is applied.[18,19] Since the Cbz groups are covalently anchored to GO, the sheets are also transported to the substrate during the course of the electrodeposition. Our group has extensively studied electrodeposited thin films by cyclic voltammetry (CV), and we found that electrodeposition by CV offers a facile control of material uniformity and thickness by simply tuning the number of cycles.[20] Another advantage is the ability to afford patterned polymer surfaces, which is easily attained by electrodeposition on a templated substrate with conductive and nonconductive regions. These electrodeposited thin films were demonstrated to have potential applications as smart, electropatterned, conductive, antibiofouling, and anticorrosion coatings.[21−23]

The electrodeposition of graphene nanomaterials had been demonstrated in the past by direct electrodeposition and by physically mixing an electroactive polymer such as poly(*N*-vinylcarbazole) and poly(3,4-ethylenedioxythiophene).[24−26] The physical interaction is mainly based on weak van der Waals forces, $\pi-\pi$ stacking, and noncovalent interactions with GO's oxygen-rich functionalities. However, the electrodeposi-

Received: January 28, 2015
Accepted: April 30, 2015
Published: April 30, 2015

DOI: 10.1021/acsami.5b00857
ACS Appl. Mater. Interfaces 2015, 7, 10266−10274

Scheme 1. (a) Synthesis Scheme of GO−Cbz and (b) Electrochemical Set-up for the Electrodeposition of GO−Cbz

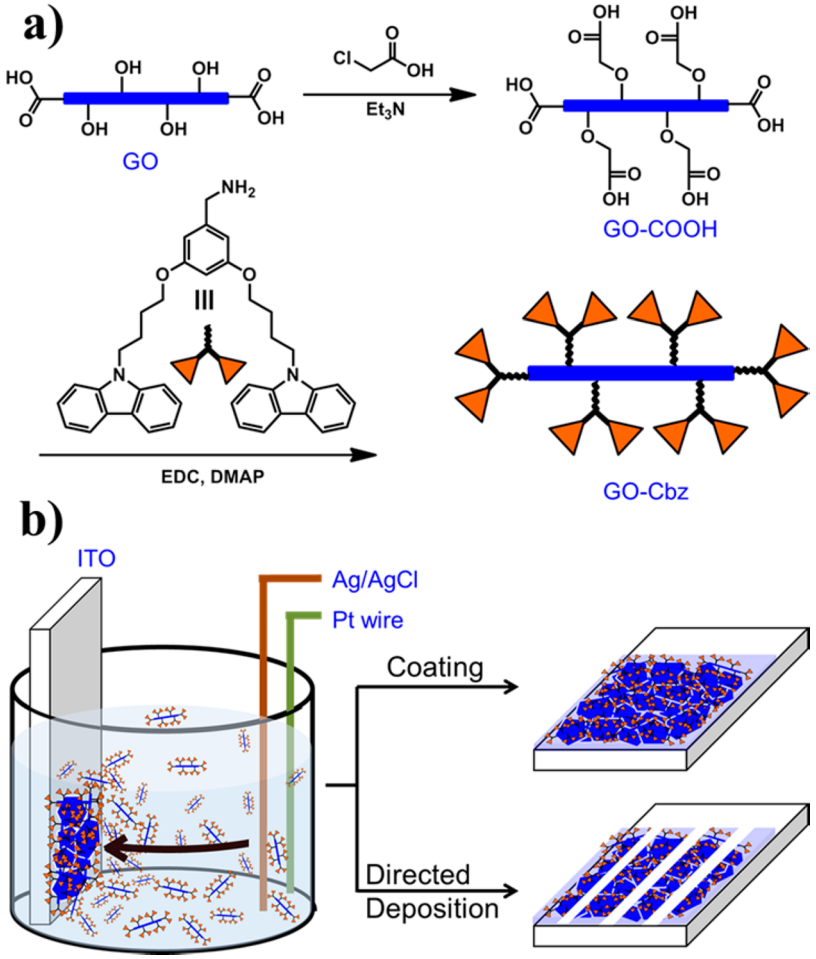

tion of graphene by covalently linked electroactive monomer is first demonstrated in this report. While noncovalent functionalization has its own benefits, covalent functionalization guarantees a strong and irreversible bond between the nanosheet and the polymer matrix.[27] It is also for this reason that we explored the potential use of GO−Cbz as a cross-linkable filler in poly(*N*-vinyl carbazole) (PVK). We hypothesized that the intermolecular cross-linking of Cbz groups from GO−Cbz and PVK will result to a nanocomposite coating with improved barrier performance for anticorrosion application.

RESULTS AND DISCUSSION

The synthesis of GO covalently tethered with Cbz group (GO−Cbz) is displayed in Scheme 1, panel a. Briefly, pristine GO was synthesized based on previously reported literature.[28] GO, a heavily oxidized form of graphene, contains oxygen-rich functional groups such as alcohols (−OH), carboxylic acids (−COOH), and epoxides (−C−O−C−), which render GO highly soluble in water. To populate the surface of GO with −COOH moieties (GO−COOH), an S_N2-type reaction with chloroacetic acid was performed. Afterwhich, a synthesized Cbz-containing molecule, we tagged as $G1CbzNH_2$, was reacted with GO−COOH by carbodiimide cross-linking chemistry. This resulted in a tethered Cbz group via the formation of an amide bond. The product was purified by dialysis and several washing−centrifugation cycles. The supernate of every wash was subjected to UV−vis spectroscopic analysis to monitor the presence of free $G1CbzNH_2$ (Figure S1, Supporting Information). The as-synthesized GO−Cbz easily dispersed in polar aprotic solvents such as N,N-dimethylformamide (DMF), acetonitrile (ACN), and dimethyl sulfoxide (DMSO). The GO−Cbz dispersions were stable for at least 3 months with slightly flocculated platelets, which were easily dispersed back to the solution by simple shaking (Figure S2, Supporting Information). The enhanced dispersion in polar organic solvents hints the successful attachment of the Cbz group to the surface of GO. A variety of spectroscopic techniques were then employed to confirm the success of the synthetic approach.

Shown in Figure 1, panel a are the UV−vis spectra of the serially diluted GO−Cbz in DMF with concentrations ranging from 1.25×10^{-1}−7.81×10^{-3} mg/mL. The absorbance at 346 nm was plotted against the concentration, which resulted in a linear Beer−Lambert plot (R^2 = 0.99925). The extinction coefficient, α, was then calculated. The α values in DMF and 1:1 ACN/DMF are 1300.77 and 1619.10 mL/mg m, respectively. To confirm the presence of Cbz groups, the UV−vis spectra of GO−Cbz and the precursors, GO and $G1CbzNH_2$, were carefully examined. As shown in Figure S3a of the Supporting Information, the absorption profile of GO is characterized by a maximum peak at 231 nm and a shoulder band at 300 nm, corresponding to the π−π^* transitions of aromatic C═C bonds and the n−π^* transitions of C═O moieties.[29] On the other hand, the prominent peaks of $G1CbzNH_2$ are ∼290, 332, and 346 nm, which are consistent

DOI: 10.1021/acsami.5b00857
ACS Appl. Mater. Interfaces 2015, 7, 10266−10274

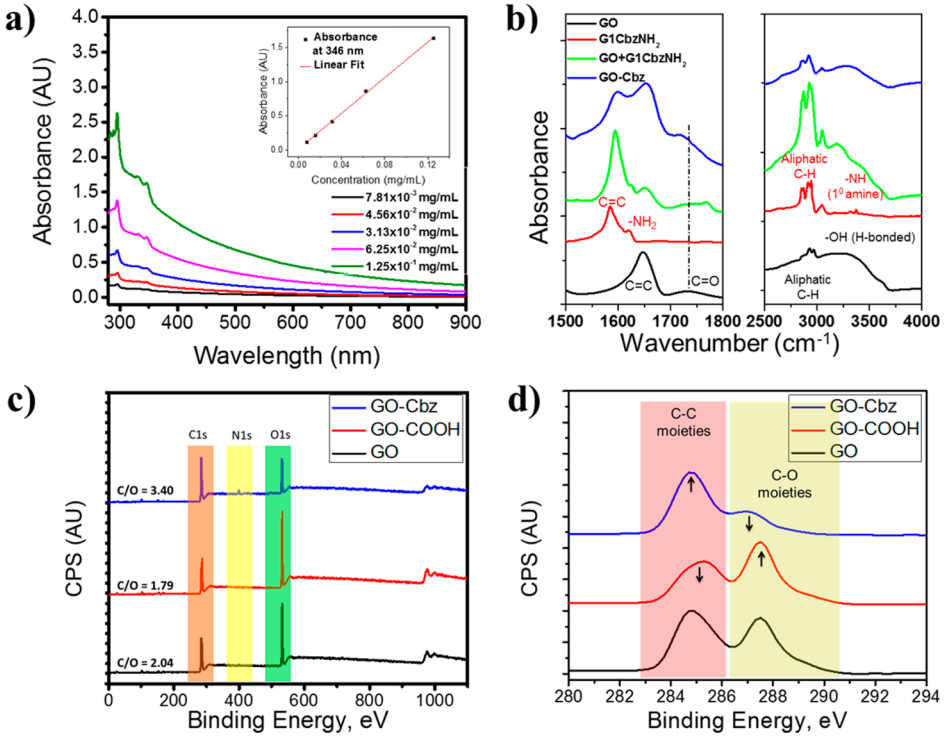

Figure 1. (a) UV−vis spectra of serially diluted GO−Cbz in DMF and Beer−Lambert plot of the absorbance at 346 nm (inset). (b) FT-IR, (c) survey and (d) high-resolution XPS spectra of synthesized materials.

with the expected absorption of Cbz and are typically assigned to the $\pi-\pi^*$ and $n-\pi^*$ transitions (Figure S3b, Supporting Information).[20] By looking at the absorption profile of GO−Cbz, it is apparent that the spectrum is similar to that of GO except for the presence of 330 and 346 nm peaks, which correspond to the signature absorption of Cbz and thus confirm the presence of Cbz to GO. To verify the covalent linkage of Cbz group, attenuated total reflectance-Fourier transform infrared (ATR-FTIR) spectroscopy was conducted (Figure 1b). Pure GO exhibits the expected C═C, C═O, aliphatic −C-H, and −OH stretches at 1648, 1732, 2856−2967, and 3000−3681 cm^{-1}, respectively. For pure $G1CbzNH_2$, C═C stretching, NH_2 bending, aliphatic −C-H, aromatic ═C−H, and N−H (1° amine) stretching were observed at 1584, 1621, 2843−2943, 3016−3047, and 3323−3375 (doublet) cm^{-1}, respectively. The spectrum of physically mixed GO +$G1CbzNH_2$ represents the combined IR peaks of both GO and $G1CbzNH_2$. However, in covalently linked GO−Cbz, the NH_2 bending and 1° amine N−H stretching disappeared, which suggests the transformation of the amine to an amide. In addition, the C═O stretch in GO, which is primarily from carboxylic acid moieties, is shifted to a lower frequency region (1717 cm^{-1}) in GO−Cbz, further confirming the presence of an amide bond. The shift is due to the weakening of the C═O due to the resonance effects with the lone pair electrons of nitrogen. The covalent linkage through amide bond is very critical so that the GO sheets will be transported to the metal substrate during electrodeposition.

X-ray photoelectron spectroscopy (XPS) was also employed to survey the elemental composition of the sample and to quantitatively determine the carbon/oxygen (C:O) ratio as a measure of the extent of functionalization. Figure 1, panels c and d display the survey and high-resolution XPS scans of GO, GO−COOH, and GO−Cbz, respectively. Both GO and GO−COOH have peaks corresponding to the binding energies of carbon and oxygen, while that of GO−Cbz contains carbon, oxygen, and nitrogen. The presence of the nitrogen peak further confirms the successful linkage of Cbz groups to the GO sheets. Quantitatively, the C:O ratio of GO was determined to be 2.04, which is consistent with the most common ratio of different GO samples studied by XPS.[28] After the reaction with chloroacetic acid, the C:O ratio of GO−COOH decreased to 1.79, as expected due to the additional oxygen from the carboxylic acid groups. As a result of the carbodiimide coupling, the C:O ratio of GO−Cbz is predicted to increase owing to the added carbon atoms from the Cbz group. The C:O ratio of GO−Cbz was determined to be 3.40. These changes in the C:O ratio are also manifested in the high-resolution scans on the spectral window of carbon where the binding energies at 284.6, 286.7, 288.0, and 288.9 eV correspond to C−C, C−O, C═O, and O−C═O moieties, respectively. A deconvoluted version of Figure 1, panel d can be found in Figure S8 of the Supporting Information.[30] High-resolution scan of N 1s from GO−Cbz also confirmed the presence of an amide group at 401.7 eV (Figure S9, Supporting Information).[31]

Meanwhile, Raman spectroscopy is indispensable in the study of graphene-based materials' electronic and structural properties, including state of doping, disorder, and surface defects. Particularly, it is useful in studying functionalized graphene and GO. The Raman spectrum of a GO sample is typically characterized by a G-band arising from the first-order scattering of the E_{2g} phonon of sp^2 carbon atoms and a disorder band or commonly known as D-band, which arises from the breathing mode of κ-point photons of A_{1g} symmetry.[32] The ratio of the intensity of D- and G-bands (I_D/I_G) can be used to characterize the level of disorder on the basal plane of GO, and this is related to the degree of functionalization (i.e., D-band

DOI: 10.1021/acsami.5b00857
ACS Appl. Mater. Interfaces 2015, 7, 10266−10274

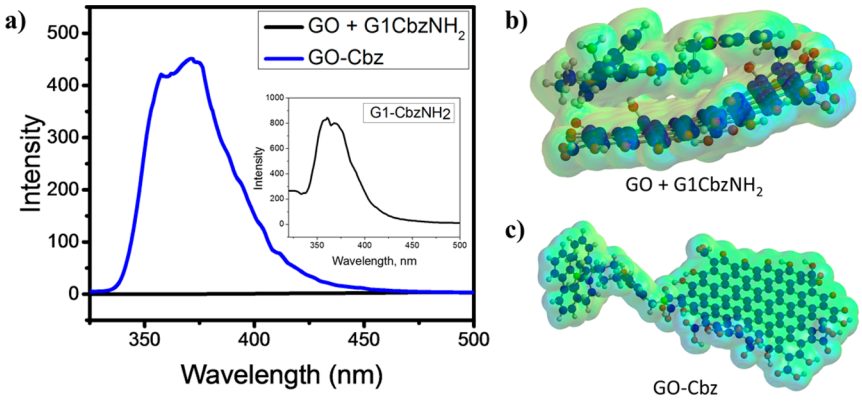

Figure 2. (a) Fluorescence spectra of GO−Cbz and physically mixed GO+G1CbzNH$_2$ at $\lambda_{excitation}$ = 295 nm (the inset is the fluorescence of pure G1CbzNH$_2$). Molecular modeling of (b) physically mixed GO and G1CbzNH$_2$ and (c) covalently bonded GO−Cbz.

increases with functionalization). The G-band and D-band of the samples centered at ∼1596 and ∼1350 cm^{-1}, respectively, are consistent with previous reports.[33] The I_D/I_G of GO is 0.75, while that of GO−COOH is 0.72 (Figure S4, Supporting Information). The minor decrease may be due to the slight reduction of GO by triethylamine (Et_3N) used during the reaction, which is also documented in another report.[34] A ∼14% increase in the I_D/I_G of GO−Cbz indicates that the Cbz group is present on the surface of GO.

The fluorescence of G1CbzNH$_2$ at $\lambda_{excitation}$ = 295 nm was also utilized to confirm the presence of Cbz groups on GO (Figure 2a, inset). It should be noted that GO itself is fluorescent at $\lambda_{excitation}$ = 400 nm with an emission band centered at ∼600 nm (Figure S5, Supporting Information). The origin of the fluorescence of GO is reported elsewhere.[30] In contrast, when excited at the same wavelength, GO−Cbz did not exhibit appreciable fluorescence. More interestingly, physically mixed GO and G1CbzNH$_2$ display no fluorescence, while covalently linked GO−Cbz exhibited the fluorescence due to the Cbz groups when excited at $\lambda_{excitation}$ = 295 nm (Figure 2a). The observed quenching in physically mixed system may well be due to strong $\pi-\pi$ stacking interactions of the preserved aromatic regions in GO and Cbz. To further understand the observed phenomenon, we performed molecular modeling of physically mixed and covalently bonded GO and G1CbzNH$_2$. The model for GO structure was based on previously reported literature where the edges were functionalized with randomly distributed 12 carboxylic acid (COOH), six carbonyl (C═O), and six hydroxyl (OH) groups.[35] Figure 2, panels b and c show the optimal minimum energy configuration when GO is physically mixed with G1CbzNH$_2$ (Energy = -2.16×10^7 kJ/mol) and when they are covalently bonded (Energy = -2.14×10^7 kJ/mol), respectively. The results of molecular modeling support the observed fluorescence quenching in physically mixed system. It can be observed that Cbz and GO tend to $\pi-\pi$ stack resulting in the loss of fluorescence of the Cbz groups (Figure 2b). The average internuclear distance of the Cbz atoms from GO atoms is around 4.5 Å, and this value falls within the length scale of $\pi-\pi$ stacking between graphene and aromatic compounds.[36,37] Such fluorescence quenching phenomenon is typically observed in physically mixed GO and aromatic compounds.[35,38,39] On the other hand, covalently bonded Cbz group tends to move far away from the sheet, which explains the conserved fluorescence (Figure 2c). More details on molecular modeling can be found in Figure S6 of the Supporting Information.

Aside from spectroscopic techniques, transmission electron microscopy (TEM) was also conducted to visualize the morphology of the resulting GO−CBz. Figure 3, panels a and b show the TEM images of GO before and after functionalization. The images depict that both GO and GO−Cbz are monolayer to few-layer exfoliated sheets with lateral dimensions in the micron regime. As shown in the figure, the functionalization apparently does not change the overall morphology of the graphene sheets,which suggests that the electronic and physical properties may have been well preserved. After GO−Cbz was carefully characterized, we then advanced to investigating its electropolymerizability by CV using indium tin oxide (ITO) or gold as the working electrode and, at the same time, the substrate (Figure 1b). Shown in Figure 3, panel c is the CV of GO−Cbz (on gold) where the peak at 0.75 V (vs Ag/AgCl) for the first cycle is attributed to the oxidation of Cbz monomer. This value is slightly lower compared to the 0.80 V (vs Ag/AgCl) oxidation potential reported for practically the same molecule as G1CbzNH$_2$.[20] This may be due to the electronic effects of the covalently linked GO nanosheet. As the number of cycles increased, the monomer oxidation peak disappeared, and a new peak at 0.9 V (vs Ag/AgCl), which is attributed to the oxidation of the dicarbazyl species, was observed.[18] The current value of this oxidation peak decreased with the succeeding cycles, which is similar to the phenomenon observed for electropolymerized PVK in dilute solution (the concentration of GO−Cbz used is 1.25×10^{-1} mg/mL).[25] One known reason for the decrease in peak current is the depletion of cross-linkable Cbz monomers of the already electrodeposited film.[25] Another explanation is the reduced electron transfer kinetics, that is, as the electropolymerization proceeds, a generally nonconducting electrodeposited GO−CBz film can act as a barrier and prevent electron transfer. The CV results of pure GO and G1CbzNH$_2$ are displayed in Figure S7 of the Supporting Information, and it should be noted that we observed no deposition of GO, while a thin film of electropolymerized G1CbzNH$_2$ was deposited onto the substrate due to its Cbz groups. Overall, the electrochemical data clearly signify successful electropolymerization and electrodeposition. In addition, the 10° increase in the water contact angle of the substrate before (63.60 ± 2.04 °) and after (73.97 ± 2.28 °) CV also verified the electrodeposition of GO−Cbz thin film (Figure 3c, inset).

Spectroscopically, one can also verify the formation of a conjugated polymer network by subjecting the film to UV−vis analysis. Figure 3, panel d shows that the film exhibits a broad

DOI: 10.1021/acsami.5b00857
ACS Appl. Mater. Interfaces 2015, 7, 10266−10274

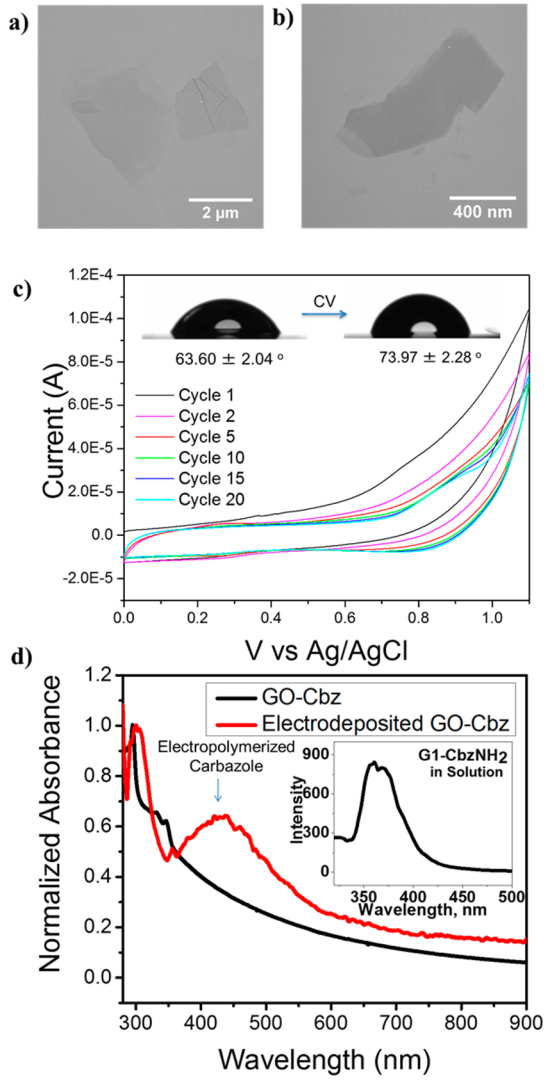

Figure 3. TEM of (a) GO and (b) GO−Cbz. (c) Cyclic voltammogram of GO−Cbz and water contact angle measurement before and after CV (inset). (d) Absorption spectra of GO−Cbz and electrodeposited GO−Cbz film; inset is the electropolymerized GO−Cbz in solution.

absorption band centered at ∼450 nm, which is typical with cross-linked Cbz.[20] We also performed UV−vis analysis to the solution left after the CV experiment, and it also showed the same absorption profile as that of the film. These are GO−Cbz sheets that were unable to electrodeposit given the applied CV conditions. As depicted in Figure 4, panel a, both inter- (green bonds) and intramolecular (light blue bonds) cross-linking can occur during electropolymerization, resulting in a conjugated polymer network. This has an important implication, and we conjecture that the GO−Cbz sheets are more structurally robust since they are covalently interconnected in a network fashion. We also expect that this hybrid film will exhibit interesting optoelectronic properties that have a great potential for the fabrication of electronic devices.[40−42]

Moreover, scanning electron microscopy (SEM) imaging was used to visualize the morphology and orientation of electrodeposited GO−Cbz sheets. Figure 4, panel b shows a wide-area SEM image of the electrodeposited GO−Cbz showing a uniform film of interdigitated, overlapping nanosheets (the lighter region of the image is the substrate that was not exposed

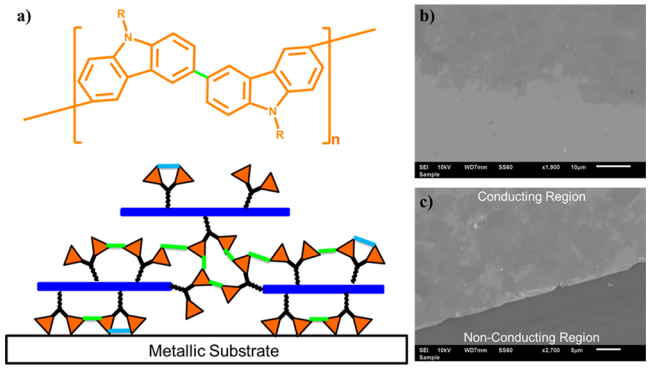

Figure 4. (a) Conjugated polymer network in the electrodeposited GO−Cbz thin film. The blue rectangles are the side-view of the nanosheets. SEM images of (b) electrodeposited GO−Cbz and (c) directed assembly on the conducting region of the substrate.

to the solution). Since Cbz groups are present in both sides of GO−Cbz, an overlapping GO−Cbz sheet is expected (Figure 4a). It is also worth noting that the sheets are generally flat with respect to the substrate. Finally, to demonstrate that the electrodeposition of GO−Cbz can be directed, we deliberately scratched a gold substrate with a razor blade to physically create nonconducting regions. Afterwhich, we electrodeposited GO−Cbz using the same CV conditions. As shown in Figure 4, panel c, the GO−Cbz sheets selectively deposit on the conducting regions, which demonstrates their promise for the fabrication of electropatterned graphene-based devices. Directed deposition on smaller features/patterns as well as the evaluation of the electronic properties of electrodeposited GO−Cbz is currently underway.

To further demonstrate the usefulness of GO−Cbz, we formulated a 1 wt % GO−Cbz in PVK matrix and used this as a nanocomposite coating. For comparison, pure PVK and 1 wt % of GO in PVK were also prepared. For a coating to be effective in preventing corrosion, it has to efficiently prevent the diffusion of the corrosive chemicals through it.[43] Currently, researchers are developing ways to effectively prevent water from diffusing through the coating either by adding 2D nanomaterials or by making the outer surface superhydrophobic.[21] PVK is an example of a conducting polymer, which can anodically protect the substrate and can form a highly conjugated network. Its performance can be drastically improved by adding 2D nanomaterials that can function as an impermeable barrier that will increase the tortuosity of the nanocomposite coating. GO, by itself, is very hydrophilic and is not compatible with the hydrophobic PVK. It is therefore imperative to functionalize the GO with a hydrophobic molecule and even better if the said molecule can actually react and be part of the conjugated polymer network.

To quantitatively measure the corrosion protection efficiency of the coatings, a potentiodynamic polarization experiment was done. Bare, PVK-coated, PVK−GO-coated, and PVK−GO−Cbz-coated stainless steel were immersed in 0.5 M NaCl solution for 36 h. The corrosion performance of the samples can be determined by analyzing the corrosion potential (E_{corr}) and the corrosion currents (I_{corr}). These parameters are extracted from the potentiodynamic polarization curves via a computer routine by specifying the cathodic and anodic branches and using nonlinear least-squares fitting method of Levenberg/Marquardt.[44] Corrosion rate (eq 1) and protection efficiencies (eq 2) are determined using the following formula:

DOI: 10.1021/acsami.5b00857
ACS Appl. Mater. Interfaces 2015, 7, 10266−10274

$$\text{Corrosion Rate} = \frac{I_{corr} x K x EW}{dA} \quad (1)$$

where I_{corr} is the corrosion current, K is the constant that defines the unit of the corrosion rate, EW is the equivalent weight in grams/equivalent, d is the density, and A is the sample area; and

$$\text{Protection Efficiency} = \frac{I_{corr,Bare} - I_{corr,Coated}}{I_{corr,Bare}} \times 100 \quad (2)$$

where $I_{corr,Bare}$ and $I_{corr,Coated}$ are the corrosion current density for uncoated and coated stainless steels, respectively.

The corrosion rates for each sample are extracted from the Tafel plots (Figure S12, Supporting Information) and are presented in Figure 5, panel a. It can be seen that the corrosion rate for bare stainless steel after 36 h of immersion is 11.25 μm/year. The corrosion rate is drastically reduced when the stainless steel is coated with PVK (1.2 μm/year). This is equivalent to 89.3% protection efficiency. The addition of GO increased the measured corrosion rate by a bit (1.59 μm/year, 85.9% protection efficiency). This is brought about by the surface energy incompatibility of the graphene oxide (which is hydrophilic) and the PVK polymer matrix (which is hydrophobic). Functionalizing the surface energy of the GO with Cbz lowers its surface energy and makes it compatible with the PVK. This is evidenced by the further decrease in the corrosion rate of PVK−GO−Cbz (0.52 μm/year). This is equivalent to 95.4% protection efficiency.

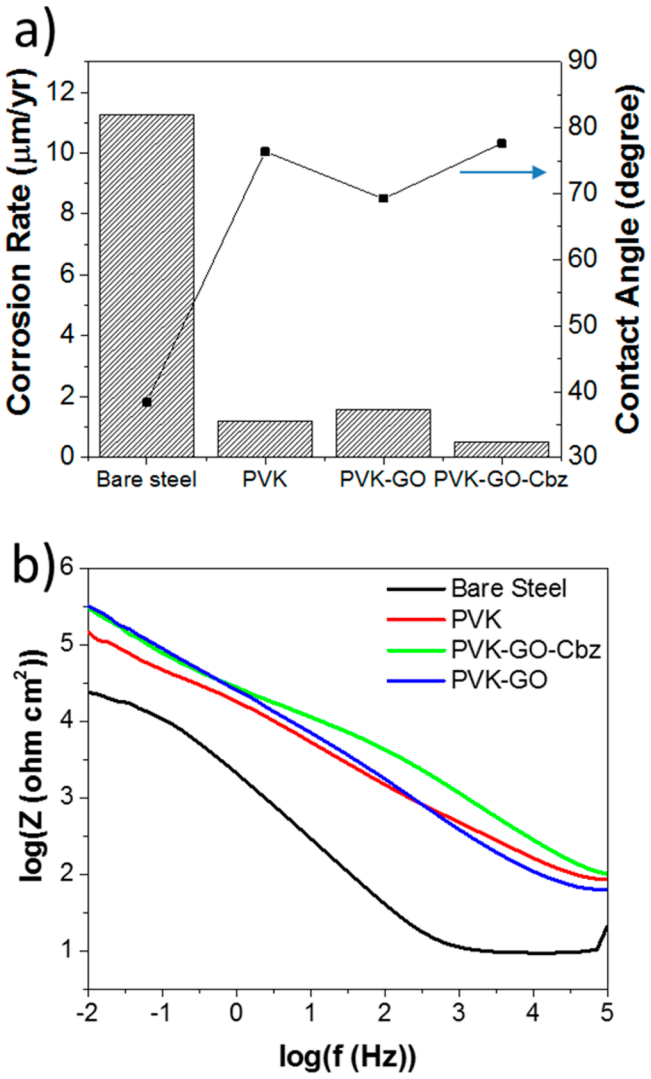

Figure 5. (a) Corrosion rate (bar) and contact angles (line) and (b) Bode magnitude plot of samples immersed in 0.5 M NaCl for 36 h.

The difference in the observed corrosion rates could be explained by the how well the water can be absorbed and reach the underlying substrate (Figure S11, Supporting Information). It is therefore expected that hydrophobic coatings can protect better than hydrophilic coatings. Figure 5, panel a shows the contact angles of the samples before immersion in 0.5 M NaCl. The bare stainless steel is the most hydrophilic with a contact angle of 38.4°. PVK-coated and PVK−GO−Cbz-coated stainless steel are both more hydrophobic (contact angles 76.4° and 77.6°, respectively) than bare stainless steel. The contact angle for PVK−GO-coated stainless steel (69.2°) is higher than bare stainless steel but less than the contact angles of the other coatings.

To better understand the superior performance of the PVK−GO−Cbz as coating, electrochemical impedance spectroscopy was employed. Impedance spectroscopy is a nondestructive method to determine parameters like the coating capacitance and resistance, which are related to the extent of water and ion absorption. This is done by applying an alternating current of 10 mV amplitude and of varying frequency from 100 kHz to 10 mHz.[45] Analysis of the impedance at frequency =1 kHz is used to qualitatively estimate the behavior of the polymer coating for corrosion protection.[46] Impedance values can be related to the capacitance and the resistance of the coating. High impedance value generally could be brought about by very low capacitance or very high resistance of the coating.[47] Large value of capacitance or low value of resistance could be brought about by (1) high extent of water absorption, high extent of formation of ionically conducting path through the coating, or (3) increase in coating delamination area.[48] It is therefore desirable for the coating to have low capacitance and high resistance. The Bode plot for all the samples is presented in Figure 5, panel b. After 36 h of immersion, the Bode magnitude plot for bare stainless steel shows a very low overall impedance value of log Z = 1.042 at 1 kHz. The impedance values for PVK- and PVK−GO-coated stainless steel are above log Z = 2.663 and 2.564 at 1 kHz, respectively. Lastly, the PVK−GO−Cbz-coated stainless steel showed the highest overall impedance value of log Z = 3.04. These results suggest that GO−Cbz is a promising material for the fabrication of nanocomposite coatings for anticorrosion application. In as little as 1 wt % GO−Cbz loading, a protection efficiency as high as 95.4% was achieved. The performance PVK−GO−Cbz nanocomposite coatings with increasing amount of GO-Cbz is being currently investigated.

CONCLUSION

A simple two-step synthetic route to afford GO nanosheets that can be readily electrodeposited on metallic substrates is demonstrated. This is based on the covalent tethering of an electroactive Cbz group to GO. The synthesized materials were characterized by spectroscopic and imaging techniques. During CV, the Cbz groups electropolymerize and carry the GO nanosheets as it electrodeposits on the substrate. It is also demonstrated that GO−Cbz selectively deposits to the conductive regions of the substrate only, which indicates its potential for the fabrication of electropatterned graphene-based

DOI: 10.1021/acsami.5b00857
ACS Appl. Mater. Interfaces 2015, 7, 10266−10274

devices. In addition, PVK−GO−Cbz nanocomposite coatings was demonstrated to be a promising material for anticorrosion application.

EXPERIMENTAL SECTION

Materials. All chemicals and organic solvents were purchased from Sigma-Aldrich, Fisher Scientific, EMD, Advanced ChemTech, and Alfa Aesar. The dialysis tubes were purchased from Thermo Fisher Scientific (3.5K MWCO) and Sigma-Aldrich (1.2−2K MWCO). Milli-Q water with resistivity value of 18.2 MΩ cm was used throughout the entire procedure involving water as solvent. USA Standard Testing Sieves No. 80 and No. 100 from Fisher Scientific were also used during the purification process. All other solvents and chemicals were used without further purification. Stainless steel foils (Alfa Aesar, Type 304) with composition Fe/Cr/Ni 70:19:11 wt % were cut into 2 cm × 1.5 cm pieces. The stainless steel substrates were polished with increasing grades of sand papers (80, 400, 600, and 1200) until mirror finish. The steel substrates were then bath sonicated in acetone for 10 min and dried with air prior to use.

Synthesis of GO. The synthesis of GO was performed based on reported literature with some modification.[28] Three grams of graphite flakes and 400 mL of concentrated H_2SO_4 were allowed to mix in a 1000 mL round-bottom flask (RBF) for 10 min. Then, 3 g of $KMnO_4$ was slowly added to the reaction mixture, which immediately turned dark green upon addition of $KMnO_4$. Three more 3 g portions of $KMnO_4$ were added to the reaction mixture after every 24 h of mixing. The reaction was stopped after the 4-day reaction period, and 120 mL (∼180 g) of the reaction mixture was mixed in 300 mL of ice−water mixture. After which, 2 mL of H_2O_2 was slowly added, which turned the dark purple solution to yellow. The solution was placed in 45 mL centrifuge tubes and was then centrifuged for 10 min at 4400 rpm. The supernate was discarded, and the sediments were washed with Milli-Q water once followed by centrifugation. The next series of purification step was performed using isopropanol until pH was neutral. The sediments were then sieved using No. 80 and No. 100 USA Standard Testing Sieves. The final sediment wash dialyzed for 3 days in isopropanol using 3.5K MWCO dialysis tube. After which, the solids were collected by centrifugation at 10 000 rpm for 30 min. Graphite oxide solids (1.120 g) were obtained by vacuum evaporation. To obtain GO, the graphite oxide solution was ultrasonicated for 10 min.

Synthesis of GO−COOH. In a 100 mL RBF, 100 mg of previously synthesized GO was dispersed in 50 mL of THF by sonication for 30 min. Then, 5 g of chloroacetic acid was added to the solution mixture cooled in an ice-bath. The reaction mixture was allowed to mix for 30 min followed by the slow addition of 4.66 g of triethylamine dissolved in THF. Then, the reaction mixture was allowed to mix for 12 h in N_2 atmosphere. The GO−COOH was collected by centrifugation of the reaction mixture at 4400 rpm for 10 min. The sediments were washed (in sequence) with water (2×), DMF, 1 M HCl, and finally water until pH was neutral. The synthesized GO−COOH was further purified by dialysis in water for 3 days.

Synthesis of G1CbzNH$_2$. See Supporting Information.

Synthesis of GO−Cbz. The carbazole moiety was tethered to GO by EDC coupling chemistry. In a 250-mL RBF, 30 mg of previously synthesized GO−COOH was dispersed in 30 mL of DMF by sonication for 30 min. Then, 150 mg of previously synthesized G1CbzNH$_2$ and 20 mg of DMAP were added to the solution mixture. The reaction components were allowed to mix thoroughly for 1 h in an ice-bath. Then, 50 mg of EDC HCl dissolved in 3 mL of DMF was slowly added to the reaction mixture using a syringe. The reaction was performed under nitrogen atmosphere. After 24 h, the reaction mixture was centrifuged for 30 min to sediment GO−Cbz. The sediments were then washed repeatedly by 50 mL portions of DMF (7×) until no more free G1CbzNH2 was detected in the supernate. Free G1CbzNH$_2$ was monitored by UV−vis absorbance spectroscopy. The final product was dialyzed in DMF for 3 days.

Electropolymerization−Electrodeposition of GO−Cbz. GO−Cbz was dispersed in 1:1 ACN/DMF to a final concentration of 1.25 × 10^{-1} mg/mL. Tetrabutylammonium hexafluorophosphate (TBAH), as a supporting electrolyte, was then added so that its final concentration was 0.1 M. The material was electrodeposited using CV with Ag/AgCl as reference electrode, Pt wire as counter electrode, and ITO or gold as the working electrode. The voltage was swept back and forth from 0−1.1 V and 0−1.5 V for gold and ITO substrates, respectively. The deposition was performed for 10−20 cycles at a rate of 50 mV/s. The resulting film was then washed with 1:1 ACN/DMF and was dried in vacuum operating at room temperature.

Corrosion Studies. The nanocomposite, PVK−GO−Cbz (1% wt), was prepared by dissolving 1 g of PVK (40 kDa) and 10 mg of GO−Cbz in 10 mL of THF. The solution was sonicated for 30 min for complete dispersion. Polished stainless steel substrates were then dip-coated onto the nancomposite solution using a dip-coater. The nanocomposite coating was then electrochemically cross-linked by CV at 50 mV/s from 0−1.2 V for 10 cycles (Figure S10, Supporting Information). The film was then dried prior to immersion in 0.5 M NaCl solution for 36 h. Potentiodynamic polarization scan (PPS) was performed by scanning from −0.05 to +0.05 V Ag/Ag+ reference electrode (3.5 M NaCl) about the open circuit potential (OCP). Electrochemical impedance spectroscopy (EIS) was performed for seven frequency decades from 10 mHz to 100 kHz with an amplitude of 10 mV with respect to the OCP. For both measurements, platinum was used as counter electrode, Ag/Ag+ in 3.5 M NaCl was used as reference electrode, and the stainless steel substrates were used as the working electrodes.

Instrumentation. The UV−vis absorbance of the starting materials as well as the electrodeposited GO−Cbz was recorded by Agilent 8453 spectrometer. ATR-FTIR spectra were also collected on a Digital FTS 7000 equipped with a HgCdTe detector. Fluorescence spectra were obtained on a PerkinElmer LS-45 luminescence spectrometer. TEM images were obtained on JEOL JEM-1200 EX electron microscope operating at 80 kV. On the other hand, SEM images were obtained on JEOL JSM 840A operating at an accelerator voltage of 10 kV. XPS analysis was conducted on a PHI Versaprobe 5000 scanning X-ray photoelectron spectrometer equipped with monochromatic Al Kα X-ray source ($h\nu$ = 1486.6 eV) with a 180° hemispherical energy analyzer. The spectra were surveyed from 0−1100 eV and were collected with pass energies of 94 eV. Moreover, high-resolution scans for carbon, oxygen, and nitrogen were also collected. The spectra were processed by Multipak V7.0.1 and deconvoluted using MagicPlot Student version 2.5. The electrodeposition experiments were performed in a conventional three-electrode cell using Autolab PGSTAT 12 potentiostat (Brinkman Instruments) controlled by GPES software.

Molecular Modeling. The molecular modeling of GO and G1CbzNH$_2$ was done using Spartan 08 program (v 1.2.0, Irvine, CA). Hartree−Fock models with 3−21 *G** were utilized for energy calculation. The model of GO was based on previously reported literature,[35] where the edge was functionalized with 12 carboxylic acid (COOH), six carbonyl (C═O), and six hydroxyl (OH) distributed randomly.

ASSOCIATED CONTENT

Supporting Information

Detailed synthesis of G1CbzNH$_2$. Additional spectroscopic studies performed for this work. Stability of GO−Cbz in DMF after 3 months. Additional information for the molecular modeling. The CV of pure GO and G1CbzNH$_2$. Deconvoluted high-resolution XPS scans. Additional data of the anticorrosion study performed. The Supporting Information is available free of charge on the ACS Publications website at DOI: 10.1021/acsami.5b00857.

AUTHOR INFORMATION

Corresponding Author

*E-mail: rca41@case.edu. Phone: 216-368-4566.

Notes

The authors declare no competing financial interest.

DOI: 10.1021/acsami.5b00857
ACS Appl. Mater. Interfaces 2015, 7, 10266−10274

■ ACKNOWLEDGMENTS

The authors acknowledge funding from DMR-1304214, NSF-1333651, and STC-0423914. The authors also acknowledge technical support from Biolin Scientific, Inc., Park AFM Systems Inc., and Keysight Technologies (formerly Agilent). Jennifer Espartero and Katrina Pangilinan are also acknowledged for their assistance.

■ REFERENCES

(1) Kim, M.; Safron, N. S.; Han, E.; Arnold, M. S.; Gopalan, P. Fabrication and Characterization of Large-Area, Semiconducting Nanoperforated Graphene Materials. *Nano Lett.* **2010**, *10*, 1125−1131.
(2) Balandin, A. A.; Ghosh, S.; Bao, W.; Calizo, I.; Teweldebrhan, D.; Miao, F.; Lau, C. N. Superior Thermal Conductivity of Single-Layer Graphene. *Nano Lett.* **2008**, *8*, 902−907.
(3) Lee, C.; Wei, X.; Kysar, J. W.; Hone, J. Measurement of the Elastic Properties and Intrinsic Strength of Monolayer Graphene. *Science* **2008**, *321*, 385−388.
(4) Bonaccorso, F.; Sun, Z.; Hasan, T.; Ferrari, A. C. Graphene Photonics and Optoelectronics. *Nat. Photonics* **2010**, *4*, 611−622.
(5) Dreyer, D. R.; Park, S.; Bielawski, C. W.; Ruoff, R. S. The Chemistry of Graphene Oxide. *Chem. Soc. Rev.* **2009**, *39*, 228.
(6) Zhu, Y.; Sun, Z.; Yan, Z.; Jin, Z.; Tour, J. M. Rational Design of Hybrid Graphene Films for High-Performance Transparent Electrodes. *ACS Nano* **2011**, *5*, 6472−6479.
(7) Ilić, A. Ž.; Budimir, D. Electromagnetic Analysis of Graphene Based Tunable Waveguide Resonators. *Microwave Opt. Technol. Lett.* **2014**, *56*, 2385−2388.
(8) Huang, Y.; Liang, J.; Chen, Y. An Overview of the Applications of Graphene-Based Materials in Supercapacitors. *Small* **2012**, *8*, 1805−1834.
(9) Dhand, V.; Rhee, K. Y.; Ju Kim, H.; Ho Jung, D. A Comprehensive Review of Graphene Nanocomposites: Research Status and Trends. *J. Nanomater.* **2013**, *2013*, 1−14.
(10) Mangadlao, J.; Santos, C.; Felipe, M. J.; Leon, C.; Rodrigues, D.; Advincula, G. On the Antibacterial Mechanism of Graphene Oxide (GO) Langmuir−Blodgett Films. *Chem. Commun.* **2015**, *15*, 2886−2889.
(11) Mangadlao, J. D.; Cao, P.; Advincula, R. C. Smart Cements and Cement Additives for Oil and Gas Operations. *J. Pet. Sci. Eng.* **2015**, *129*, 63−76.
(12) Cote, L. J.; Kim, F.; Huang, J. Langmuir−Blodgett Assembly of Graphite Oxide Single Layers. *J. Am. Chem. Soc.* **2009**, *131*, 1043−1049.
(13) Choi, W.; Choi, J.; Bang, J.; Lee, J.-H. Layer-by-Layer Assembly of Graphene Oxide Nanosheets on Polyamide Membranes for Durable Reverse-Osmosis Applications. *ACS Appl. Mater. Interfaces* **2013**, *5*, 12510−12519.
(14) Jeon, H. G.; Huh, Y. H.; Yun, S. H.; Kim, K. W.; Lee, S. S.; Lim, J.; An, K.-S.; Park, B. Improved Homogeneity and Surface Coverage of Graphene Oxide Layers Fabricated by Horizontal-Dip-Coating for Solution-Processable Organic Semiconducting Devices. *J. Mater. Chem. C* **2014**, *2*, 2622.
(15) Moon, I. K.; Kim, J. I.; Lee, H.; Hur, K.; Kim, W. C.; Lee, H. 2D Graphene Oxide Nanosheets as an Adhesive Over-Coating Layer for Flexible Transparent Conductive Electrodes. *Sci. Rep.* **2013**, *3*, 1112.
(16) An, S. J.; Zhu, Y.; Lee, S. H.; Stoller, M. D.; Emilsson, T.; Park, S.; Velamakanni, A.; An, J.; Ruoff, R. S. Thin Film Fabrication and Simultaneous Anodic Reduction of Deposited Graphene Oxide Platelets by Electrophoretic Deposition. *J. Phys. Chem. Lett.* **2010**, *1*, 1259−1263.
(17) Pangilinan, K. D.; Santos, C. M.; Estillore, N. C.; Rodrigues, D. F.; Advincula, R. C. Temperature-Responsiveness and Antimicrobial Properties of CNT−PNIPAM Hybrid Brush Films. *Macromol. Chem. Phys.* **2013**, *214*, 464−469.
(18) Ambrose, J. F.; Nelson, R. F. Anodic Oxidation Pathways of Carbazoles. *J. Electrochem. Soc.* **1968**, *115*, 1159.
(19) Inzelt, G. Formation and Redox Behavior of Polycarbazole Prepared by Electropolymerization of Solid Carbazole Crystals Immobilized on an Electrode Surface. *J. Solid State Electrochem.* **2003**, *7*, 503−510.
(20) Felipe, M. J.; Dutta, P.; Pernites, R.; Ponnapati, R.; Advincula, R. C. Electropolymerized Bioresistant Coatings of OEGylated Dendron Carbazoles: Design Parameters and Protein Resistance SPR Studies. *Polymer* **2012**, *53*, 427−437.
(21) De Leon, A. C. C.; Pernites, R. B.; Advincula, R. C. Superhydrophobic Colloidally Textured Polythiophene Film as Superior Anticorrosion Coating. *ACS Appl. Mater. Interface* **2012**, *4*, 3169−3176.
(22) Foster, E. L.; De Leon, A. C. C.; Mangadlao, J.; Advincula, R. Electropolymerized and Polymer Grafted Superhydrophobic, Superoleophilic, and Hemiwicking Coatings. *J. Mater. Chem.* **2012**, *22*, 11025−11031.
(23) Mangadlao, J.; Leon, C.; Felipe, M. J.; Advincula, G. Electrochemical Fabrication of Graphene Nanomesh via Colloidal Templating. *Chem. Commun.* **2015**, *51*, 7629−7632.
(24) Chen, L.; Tang, Y.; Wang, K.; Liu, C.; Luo, S. Direct Electrodeposition of Reduced Graphene Oxide on Glassy Carbon Electrode and its Electrochemical Application. *Electrochem. Commun.* **2011**, *13*, 133−137.
(25) Pernites, R.; Vergara, A.; Yago, A.; Cui, K.; Advincula, R. Facile Approach to Graphene Oxide and Poly(N-vinylcarbazole) Electropatterned Films. *Chem. Commun.* **2011**, *47*, 9810−9812.
(26) Si, W.; Lei, W.; Zhang, Y.; Xia, M.; Wang, F.; Hao, Q. Electrodeposition of Graphene Oxide Doped Poly(3,4-ethylenedioxythiophene) Film and Its Electrochemical Sensing of Catechol and Hydroquinone. *Electrochim. Acta* **2012**, *85*, 295−301.
(27) Naebe, M.; Wang, J.; Amini, A.; Khayyam, H.; Hameed, N.; Li, L. H.; Chen, Y.; Fox, B. Mechanical Property and Structure of Covalent Functionalized Graphene/Epoxy Nanocomposites. *Sci. Rep.* **2014**, *4*, 4375.
(28) Dimiev, A.; Kosynkin, D. V.; Alemany, L. B.; Chaguine, P.; Tour, J. M. Pristine Graphite Oxide. *J. Am. Chem. Soc.* **2012**, *134*, 2815−2822.
(29) Paredes, J. I.; Villar-Rodil, S.; Martínez-Alonso, A.; Tascón, J. M. D. Graphene Oxide Dispersions in Organic Solvents. *Langmuir* **2008**, *24*, 10560−10564.
(30) Shang, J.; Ma, L.; Li, J.; Ai, W.; Yu, T.; Gurzadyan, G. G. The Origin of Fluorescence from Graphene Oxide. *Sci. Rep.* **2012**, *2*, 792.
(31) Kim, H. J.; Bae, I.-S.; Cho, S.-J.; Boo, J.-H.; Lee, B.-C.; Heo, J.; Chung, I.; Hong, B. Synthesis and Characteristics of NH_2-functionalized Polymer Films To Align and Immobilize DNA Molecules. *Nanoscale Res. Lett.* **2012**, *7*, 1−7.
(32) Zhu, C.; Guo, S.; Fang, Y.; Dong, S. Reducing Sugar: New Functional Molecules for the Green Synthesis of Graphene Nanosheets. *ACS Nano* **2010**, *4*, 2429−2437.
(33) Kudin, K. N.; Ozbas, B.; Schniepp, H. C.; Prud'homme, R. K.; Aksay, I. A.; Car, R. Raman Spectra of Graphite Oxide and Functionalized Graphene Sheets. *Nano Lett.* **2008**, *8*, 36−41.
(34) Gurunathan, S.; Woong Han, J.; Kim, J. Green Chemistry Approach for the Synthesis of Biocompatible Graphene. *Int. J. Nanomed.* **2013**, *8*, 2719−2732.
(35) Basiuk, E. V.; Martínez-Herrera, M.; Álvarez-Zauco, E.; Henao-Holguín, L. V.; Puente-Lee, I.; Basiuk, V. A. Noncovalent Functionalization of Graphene with a Ni(ii)−Tetraaza[14]annulene Complex. *Dalton Trans.* **2014**, *43*, 7413−7428.
(36) Martinez, C. R.; Iverson, B. L. Rethinking the Term "Pi-Stacking". *Chem. Sci.* **2012**, *3*, 2191−2201.
(37) Rochefort, A.; Wuest, J. D. Interaction of Substituted Aromatic Compounds with Graphene. *Langmuir* **2008**, *25*, 210−215.
(38) Wang, Z.; Huang, P.; Bhirde, A.; Jin, A.; Ma, Y.; Niu, G.; Neamati, N.; Chen, X. A Nanoscale Graphene Oxide−Peptide Biosensor for Real-Time Specific Biomarker Detection on the Cell Surface. *Chem. Commun.* **2012**, *48*, 9768−9770.
(39) Yang, X.; Wang, Y.; Huang, X.; Ma, Y.; Huang, Y.; Yang, R.; Duan, H.; Chen, Y. Multifunctionalized Graphene Oxide Based

DOI: 10.1021/acsami.5b00857
ACS Appl. Mater. Interfaces 2015, 7, 10266−10274

Anticancer Drug-Carrier with Dual-Targeting Function and pH-Sensitivity. *J. Mater. Chem.* **2011**, *21*, 3448−3454.
(40) Wu, C.; Li, F.; Guo, T.; Kim, T. W. Controlling Memory Effects of Three-Layer Structured Hybrid Bistable Devices Based on Graphene Sheets Sandwiched between Two Laminated Polymer Layers. *Org. Electron.* **2012**, *13*, 178−183.
(41) Zhang, B.; Chen, Y.; Zhuang, X.; Liu, G.; Yu, B.; Kang, E.-T.; Zhu, J.; Li, Y. Poly(N-vinylcarbazole) Chemically Modified Graphene Oxide. *J. Polym. Sci., Part A: Polym. Chem.* **2010**, *48*, 2642−2649.
(42) Zhang, Q.; Pan, J.; Yi, X.; Li, L.; Shang, S. Nonvolatile Memory Devices Based on Electrical Conductance Tuning in Poly(N-vinylcarbazole)−Graphene Composites. *Org. Electron.* **2012**, *13*, 1289−1295.
(43) Weng, C.-J.; Chang, C.-H.; Peng, C.-W.; Chen, S.-W.; Yeh, J.-M.; Hsu, C.-L.; Wei, Y. Advanced Anticorrosive Coatings Prepared from the Mimicked Xanthosoma Sagittifolium-Leaf-Like Electroactive Epoxy with Synergistic Effects of Superhydrophobicity and Redox Catalytic Capability. *Chem. Mater.* **2011**, *23*, 2075−2083.
(44) Bhardwaj, M.; Balasubramaniam, R. A New Method for Determining Kinetic Parameters by Simultaneously Considering All the Independent Conditions at an Overpotential in Case of Hydrogen Evolution Reaction Following Volmer−Heyrovsky−Tafel Mechanism. *Int. J. Hydrogen Energy* **2008**, *33*, 248−251.
(45) Amirudin, A.; Thieny, D. Application of Electrochemical Impedance Spectroscopy To Study the Degradation of Polymer-Coated Metals. *Prog. Org. Coat.* **1995**, *26*, 1−28.
(46) Rammelt, U.; Reinhard, G. Application of Electrochemical Impedance Spectroscopy (EIS) for Characterizing the Corrosion-Protective Performance of Organic Coatings on Metals. *Prog. Org. Coat.* **1992**, *21*, 205−226.
(47) Kannan, M. B.; Gomes, D.; Dietzel, W.; Abetz, V. Polyoxadiazole-Based Coating for Corrosion Protection of Magnesium Alloy. *Surf. Coat. Technol.* **2008**, *202*, 4598−4601.
(48) Mansfeld, F. Use of Electrochemical Impedance Spectroscopy for the Study of Corrosion Protection by Polymer Coatings. *J. Appl. Electrochem.* **1995**, *25*, 187−202.

DOI: 10.1021/acsami.5b00857
ACS Appl. Mater. Interfaces 2015, 7, 10266−10274